Chemical Engineering Journal 160 (2010) 899–908

Contents lists available at ScienceDirect

Chemical Engineering Journal

journal homepage: www.elsevier.com/locate/cej

Carbon nanofiber based catalyst supports to be used in microreactors: Synthesis and characterization

D.B. Thakur[a], R.M. Tiggelaar[b], J.G.E. Gardeniers[b], L. Lefferts[a], K. Seshan[a,*]

[a] Catalytic Processes and Materials, MESA+ Institute for Nanotechnology, University of Twente, P.O. BOX 217, 7522 AE Enschede, The Netherlands
[b] Mesoscale Chemical Systems, MESA+ Institute for Nanotechnology, University of Twente, P.O. BOX 217, 7522 AE Enschede, The Netherlands

ARTICLE INFO

Article history:
Received 14 July 2009
Received in revised form
17 December 2009
Accepted 6 January 2010

Keywords:
Carbon nanofibers
Structured catalyst support
Nickel thin-film
Growth parameters
Microreactors

ABSTRACT

Carbon nanofiber (CNF) layers have been synthesized on flat fused silica and silicon substrates, as well as inside flow channels of silicon-technology based microreactors by thermal catalytic chemical vapor deposition of ethylene using nickel thin-film catalyst. These CNF layers are to be used as structured catalyst support. The influence of the ethylene concentration and addition of hydrogen to the carbon-containing gas on the morphology of CNF layers was studied. Very low amount of CNFs were produced at low ethylene concentrations (<25%) due to the restricted supply of carbon species. Addition of hydrogen during the CNF growth resulted in significant enhancement of the CNF-yield, producing thicker layers of CNFs and CNFs with smaller diameters. Channels containing silicon micropillars covered with these CNFs have a significantly enhanced surface-to-volume ratio compared to bare microreactor channels (3–4 orders of magnitude). Deposition of well-distributed platinum nanoparticles was carried out on these CNF layers, exemplifying their functionality as structured catalyst support to be used in microreactors.

1. Introduction

Currently, there is a growing interest in the design and use of microscale reactors as efficient systems for the synthesis of specific, low volume, high value fine and specialty chemicals such as pharmaceuticals and additives. Microreactors are small-scale fluidic systems comprising fluid channels with lengths in the millimeter-to-centimeter range and cross-sectional dimensions in the range sub-micrometer to sub-millimeter [1,2]. Due to these small dimensions microreactors have high surface-to-volume ratios (in the order 10^4 m^2/m^3) that result in improved heat and mass transfer characteristics, which are critical for carrying out chemical reactions efficiently [1–4]. Enhanced heat transfer rates prevent thermal runaway during reactions (*i.e.* safer operation), and improved mass transfer rates (*i.e.* small diffusion distances) avoid issues as concentration gradients and secondary reactions resulting in bye products/waste [5]. Various industries can directly benefit from the use of microreactor technology: an example is the fine chemicals industry which often involves multiphase reactions (gas–liquid–solid), where the solid phase is mostly a catalyst. These catalytic reactions, however, pose a substantial challenge in achieving efficient contact and mass transfer between different phases [6–8].

The integration of a solid catalytic phase (heterogeneous catalyst) in microreactors is a challenging task. Conventionally, it is achieved in two ways, *i.e.* (i) by using a micro packed-bed of powdered catalyst [9–11], or (ii) by using a thin layer of catalyst coated on the inner wall of a microchannel [12–14]. However, a powdered catalyst packed-bed might result in high pressure drops along the length of reaction-channel, whereas a thin catalyst coating usually fails to utilize the entire volume of the reactor channel effectively. Most of these problems can be overcome by introducing nanoscale structural features in the microchannels. For microsystems various possibilities have been explored, such as use of porous anodic alumina layers [15,16], walls coated with porous materials such as zeolites [17,18], and black or porous silicon [19,20]. An exciting option in this regard is the use of rigid, porous and orderly arranged catalyst supports based on carbon nanostructures, such as carbon nanofibers, onto which a metallic catalytic active phase (*e.g.* platinum (Pt) or palladium (Pd) nanoparticles) can be deposited.

1.1. Theory

Since the landmark paper by Iijima in 1991 [21], carbon nanostructured materials such as carbon nanofibers (CNFs) and carbon nanotubes (CNTs) have received a tremendous interest. This is due to their exceptional mechanical, electrical, physical and chemical characteristics [22–25], which makes them attractive for variety of applications. Applications of CNFs and CNTs include emitters for field emission displays (FED) [26], composite reinforcing materi-

* Corresponding author. Tel.: +31 53 489 3254; fax: +31 53 489 4683.
E-mail address: k.seshan@utwente.nl (K. Seshan).

1385-8947/$ – see front matter © 2010 Elsevier B.V. All rights reserved.
doi:10.1016/j.cej.2010.01.005

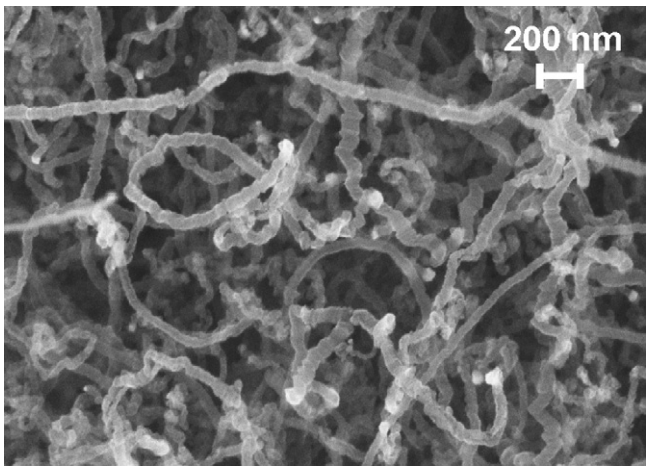

Fig. 1. High-resolution SEM image of entangled ('jungle') carbon nanofibers [54].

als [27], hydrogen storage [28], bio- and chemical sensors [29,30], nano- and microelectronic devices [31,32], and as a catalytic support electrodes for fuel cells [33,34].

Carbon nanostructures offer numerous advantages as catalyst supports for chemical reactions *viz.*, (i) corrosion resistance to acid or base medium, (ii) high length (μm)-to-diameter (nm) ratio and high surface area, (iii) absence of micro porosity, (iv) possibility to tune the surface chemistry, and (iv) easy recovery of precious metal catalysts supported on them by simply burning the carbon skeleton [35–37]. A range of structured materials including monoliths [38], foams [37,39–41], filters [42], glass and carbon fibers [43,44] and cloths [45] has been used for the synthesis of CNF layers. The small dimensions of carbon nanostructures and the above-mentioned advantages as catalyst support motivate integration of CNFs and/or CNTs as structured catalyst support layers in miniaturized reaction systems, *i.e.* microreactors.

The synthesis of carbon nanostructures can be achieved *via* arc discharge [46], laser ablation [47] and chemical vapor deposition (CVD) methods (*e.g.* catalytic thermal CVD and plasma enhanced CVD) [48–50]. The catalytic thermal chemical vapor deposition (C-TCVD) method is a versatile technique and a relatively cheap method for large-scale applications [51–53], and therefore most often used for CNF-synthesis. The C-TCVD method utilizes decomposition of carbon-containing gases on catalytically active components such as transition metals such as nickel (Ni), cobalt (Co) and iron (Fe) or alloys of these materials (due to their ability to dissolve carbon/or form metal carbides) [49]. Hydrocarbon gases such as methane (CH_4), acetylene (C_2H_2), ethylene (C_2H_4), ethane (C_2H_6), or other C-sources as carbon monoxide (CO) or synthesis gas ($CO + H_2$) can be used to obtain CNF growth on these metal catalysts at temperatures between 400 and 1000 °C [51].

There are, however, critical issues which have to be addressed in order to obtain microreactors of which the flow channels are filled with an efficient CNF-based catalyst support, *i.e.* a layer of entangled CNFs 'jungle' as shown in Fig. 1 [54]. These are, (i) deposition of well adhered metal catalyst layer (*e.g.* Ni [12,49]) required for the synthesis of CNFs, (ii) good attachment of the synthesized CNF layer to the microchannel, (iii) obtaining controlled CNF growth, (iv) efficient utilization of the microchannel volume to obtain a high surface area for active metal deposition, and (v) preparing CNF-based catalyst layer by depositing stable and well dispersed active metal particles.

In previous work issues concerning the preparation of stable metallic layers for CNF-synthesis (*i.e.* Ni-based thin-films) on fused silica substrates as well as improvement of the attachment of CNF-coatings were addressed [54,55]. It was demonstrated that presence of a metal adhesion layer is necessary for the stability of the deposited Ni thin-film on the substrate, and the choice of a proper adhesion material (*i.e.* TiW and Ta) not only improves the attachment of synthesized CNF-coating, but also helps to tune morphological properties such as the diameter of CNFs.

In this work new results are presented to probe the influence of some of the crucial CNF growth parameters on their growth as well as the resulting morphology. Furthermore, an approach to efficiently utilize the microchannel volume for reaction is shown, *i.e.* micromachined channels filled with arrays of pillars covered with a CNF-coating, as shown in Fig. 2. The growth parameters investigated in this work are the hydrocarbon gas concentration and the addition of hydrogen during CNF-synthesis. A systematic approach has been followed to obtain knowledge on CNF growth *via* the use of a flat substrate-based model system mimicking the channel surfaces, which is then translated towards structured microchannels into which CNFs have to be anchored as catalyst support. CNF layers were functionalized as catalytic support by depositing an active metal, such as Pt, by pulsed-laser deposition.

2. Experimental

2.1. Preparation of nickel-based thin-films on flat fused silica and silicon substrates

Ni-based thin-films for the synthesis of CNFs were deposited on fused silica substrates (Corning, UV Grade 7980F; diameter 100 mm, thickness 500 ± 25 μm, roughness as-fabricated <1 nm) and oxidized silicon substrates (standard p-type silicon substrates (⟨1 0 0⟩-oriented, p-type, resistivity 5–10 Ω cm, 100 mm diameter, thickness 525 μm, single side polished; Okmetic, Finland - ~250 nm SiO_2 using steam oxidation).

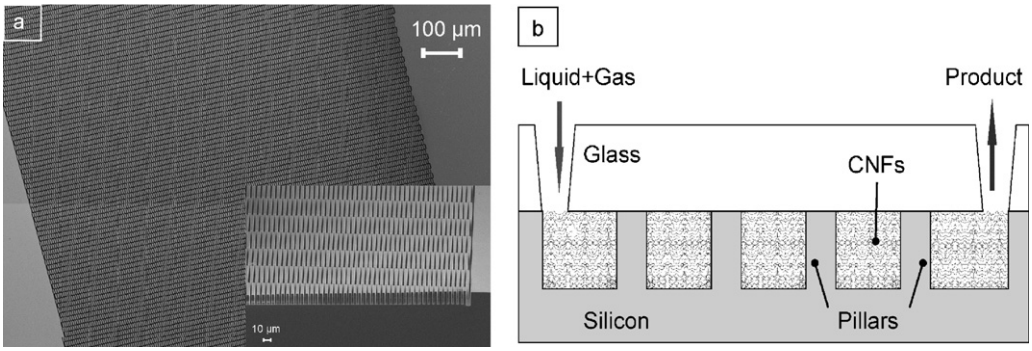

Fig. 2. (a) SEM image of array of micromachined silicon pillars; (b) schematic cross-section of pillared microchannel with CNFs that act as catalyst support (not on scale).

Post to nitric acid cleaning sequence and lithography, deposition of metals was done *via* evaporation (Ni/Ta) and sputtering (Ni/TiW). Experimental details of these procedures can be found elsewhere [54]. The thickness of the deposited adhesion layer was 10 nm, with on top 25 nm nickel. Finally, the substrates with the thin metal films were diced into samples of 1 cm × 1 cm, with a centered 8 mm × 8 mm area of metal thin-film.

2.2. Fabrication of microchannels containing ordered arrays of pillars

Microchannels of 30 × 1 mm containing ordered arrays of elongated hexagonal pillars were defined in standard p-type silicon substrates (⟨1 0 0⟩-oriented, p-type, resistivity 5–10 Ω cm, 100 mm diameter, thickness 525 μm, single side polished; Okmetic, Finland). Prior to processing, the substrates were cleaned by immersion in fuming 100% nitric acid and boiling 69% nitric acid followed by quick dump rinsing in de-mineralized water and dry spinning. With standard UV-lithography microchannels with pillars (pillar specifications: length 15 μm, width 3 μm, and spacing 3 μm) were defined in photoresist, which was postbaked for 30 min at 120 °C (in air) after development. The photoresist acted as a masklayer during deep reactive ion etching (DRIE; Adixen AMS 100DE) of silicon with a Bosch process, *i.e.* a cyclic process which uses sulfur hexafluoride for etching of silicon and octafluorocyclobutane for sidewall passivation. The height of the pillars (thus the depth of the channel) was ∼20 μm. Post to etching the mask was stripped with an oxygen plasma and immersion in 100% nitric acid, followed by rinsing and drying. Fluorocarbons resulting from the DRIE process were removed by a wet oxidization step, followed by immersion in 1% hydrofluoric acid, rinsing in DI-water and drying. A second wet oxidation step (45 min, 1000 °C) was used to deposit a ∼250 nm thick SiO_2 layer on the etched microchannel. A thin-film of Ni/Ta (25 nm/10 nm) was deposited on the micropillars using electron-beam evaporation (Balzers BAK600 system) in combination with a home-built stainless-steel shadowmask, using identical settings as for evaporation of Ni/Ta films on flat substrates. Finally, the substrates were diced into samples of 40 mm × 3 mm.

2.3. CNF layer synthesis

2.3.1. Reduction pretreatment

Prior to CNF-synthesis the nickel-based thin-film samples, both flat substrates and microchannels with arrays of pillars, were first cleaned ultrasonically in acetone (5 min, Branson 200 ultrasonic cleaner) to remove organic contaminants, followed by washing with flowing deionized water (25 °C) and dried with pressurized technical air. Subsequently, the samples were reduced in a mixture of 20 vol.% H_2 in N_2 (99.999%, INDUGAS) with total flow rate of 50 mL/min, while increasing the temperature to 500 °C (ramp up 5 °C/min) and maintained at 500 °C for 2 h. This pretreatment is essential for the dewetting of the Ni thin-film to produce nanoparticles which act as nucleation sites for CNF growth. After cooling down to room temperature, the samples were transferred to the CNF-synthesis set-up for carrying out CNF-synthesis.

2.3.2. CNF growth

CNF-synthesis was performed in a quartz reactor heated by a vertical furnace and horizontal furnace for flat substrates and microreactor chips, respectively. The use of different furnaces was simply for the better handing of samples with different sizes. Flat fused silica samples with Ni-based thin-films were heated in N_2 in vertical furnace from room temperature to 700 °C at a rate of 5 °C/min, and at 700 °C exposed to a reactive gas mixture of C_2H_4 in N_2 (99.95%, PRAXAIR) and/or H_2 at a total flow rate of 100 mL/min. The reaction time at this temperature was one hour, after which the samples were cooled down in N_2 to room temperature. Two different sets of experiments were carried out to probe the influence of growth parameters on CNF growth and their morphology: (i) variation of ethylene concentration (5–15–25–30 vol.%) balanced with N_2 at 100 mL/min total flow rate, and (ii) H_2 addition during CNF growth (6.25–12.5–25 vol.%), using 25 vol.% C_2H_4 balanced with N_2 at 100 mL/min total flow rate. These hydrogen concentrations were chosen to obtain three different H_2/C_2H_4 ratios, *viz.* 1:4, 1:2 and 1:1. The amount of carbon deposited on each sample was determined by measuring the increase in weight.

CNFs were synthesized inside microchannels with arrays of pillars by positioning samples on a quartz boat in a horizontal quartz reactor heated by an outer furnace. The samples were heated in N_2 from room temperature to 635 °C at a rate of 5 °C/min, and at 635 °C exposed to a reactive gas mixture of C_2H_4 in N_2 (99.95%, PRAXAIR) and H_2 (0 and 6.25 vol.%) at a total flow rate of 100 mL/min. The reaction time was one hour or 2 h, after which the samples were cooled down in N_2 to room temperature.

2.4. Active metal deposition on CNF layers

Platinum (Pt) film was deposited by pulsed-laser deposition (PLD) using a KrF excimer laser beam with a wavelength of 248 nm. The spot size of the laser beam was 1.95 mm^2, with an energy density of 4.5 J/cm^2. A Pt target with a density of 21.45 g/cm^3 (99.99%) was used. The distance between the platinum target and CNF-coated samples was 42 mm. The deposition rate was 0.04 nm/pulse, and the film thickness achieved on a fiber body was about 2.5 nm, which corresponds to ∼3.5 wt.% loading of Pt (based on weight of deposited CNF layer). The deposition was carried out at room temperature in Ar atmosphere at a pressure of 0.01 mbar. The Pt film was further annealed at 500 °C for 2 h in N_2 atmosphere for thermal disintegration of the film to generate well dispersed nanoparticles.

2.5. Characterization

The morphology of the synthesized CNF-coatings was investigated by scanning electron microscopy (HRSEM; LEO 1550). Cross-sectional SEM analysis was performed on samples after cleaving manually with pliers. In case of CNF layers synthesized inside pillared microchannels, ultrasonication in water (5 min, Branson 200) was used to verify the attachment of CNF layers, followed by drying and SEM-inspection.

3. Results and discussion

Incorporation of a metal adhesion layer ensures good adhesion of the Ni thin-film to the fused silica substrate. Previously, it is shown that the use of Ta or TiW underneath Ni resulted in well-attached CNF-coatings, even under intense fluid flow conditions (*i.e.* flow in the m/s range). Moreover, the type of adhesion material influences the diameter of the fibers constituting this coating: Ta yields fibers with smaller diameter than TiW [54]. When synthesized in microchannels, control of the morphology of CNFs – *i.e.* average diameter of CNFs and CNF layer thickness – is important to be able to optimally fill the volume of the microchannels (efficient catalyst support), for example the spacing between pillars (see Fig. 2b).

It is known from literature that a variety of growth parameters can influence the morphology of CNFs. Important parameters are the growth catalyst, synthesis temperature, type of C-source gas and its concentration, gas velocity and partial pressures, growth duration and addition of hydrogen during CNF growth [53,56–60]. Overall, the most crucial parameters in CNF-synthesis are the concentration and flow rate of the C-source, the concentration of hydrogen, and the synthesis temperature [53]. In this work the

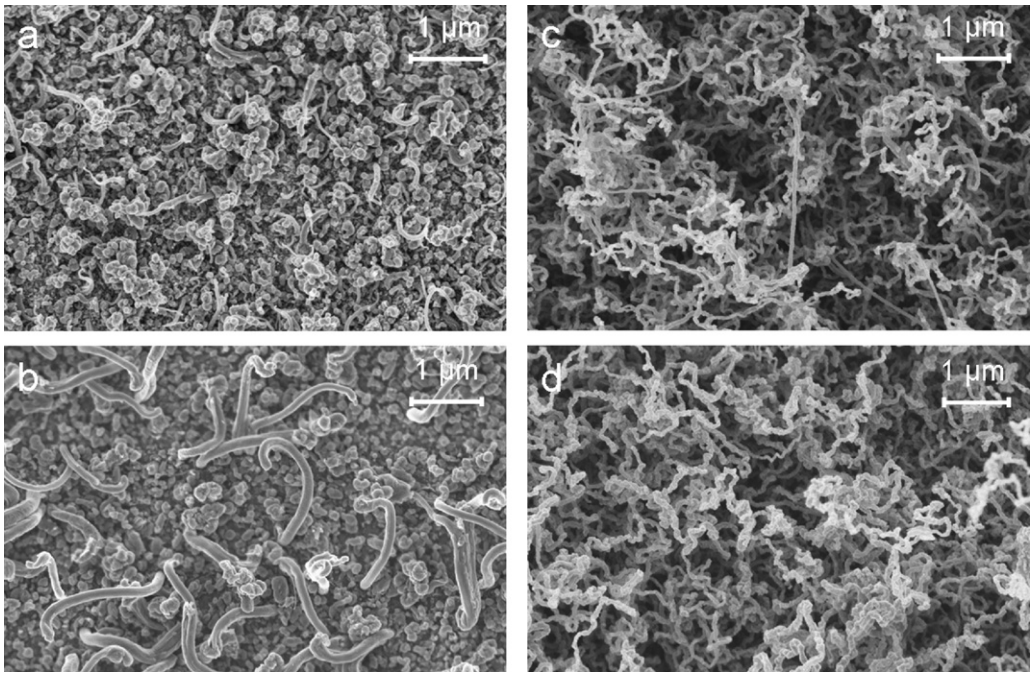

Fig. 3. Top-view SEM images illustrating CNF morphology for different C_2H_4 concentrations (total flow rate of 100 mL/min; fused silica samples with 25 nm Ni and 10 nm TiW): (a) 5 vol.%, (b) 15 vol.%, (c) 25 vol.%, and (d) 30 vol.%.

influence ethylene concentration and addition of hydrogen on the C-TCVD CNF growth process is studied.

3.1. Influence of growth parameters on CNF-synthesis

3.1.1. Ethylene concentration

Fused silica samples with a metal thin-film of Ni/TiW were exposed to the C-TCVD process. The ethylene concentration in the reacting mixture was varied from 5 vol.% to 30 vol.%. Fig. 3 shows top-view SEM images of the samples for increasing C_2H_4 concentrations, and Table 1 presents the amount of deposited carbon deposited as well as the average CNF diameters CNFs for different concentrations of C_2H_4. The SEM images clearly show a change in the CNF morphology as a function of the C_2H_4 concentration. For 5 vol.% C_2H_4 nearly no CNF growth is observed (Fig. 3a): only a small amount of carbon is deposited with a scattered growth of CNF resembling structures. For 15 vol.% C_2H_4 a small amount of CNFs is found with an average diameter of 150 nm (Fig. 3b). In case of 25 and 30 vol.% C_2H_4 rather large amounts of uniform layers of entangled CNFs are seen (Fig. 3c and d). The amount of deposited carbon increased with increasing C_2H_4 concentration, but seems to level off at high C_2H_4 concentrations. Cross-sectional SEM-images (not shown here) revealed the presence of a 'dense' C-layer at the metal interface (*i.e.* underneath the open, entangled jungle CNF layer). In Fig. 4 the thicknesses of this 'dense' C-layer as well as the CNF layer are plotted as a function of the C_2H_4 concentration. For increasing ethylene concentrations the thickness of both layers increases, and only for C_2H_4 concentrations exceeding 15 vol.% significant CNF-growth is visible (for lower concentrations only deposition of carbonaceous species).

From literature it is known that the concentration of the C-source gas influences both the CNF growth rate and the rate of deactivation [56]. At lower concentrations insufficient supply of C-species restricts deposition of carbon and hence the CNF growth rate, whereas at very high concentrations the rate of deposition of carbon on the nickel particles is becoming so high that carbon consumption *via* CNF growth is not able to keep up. As a consequence, excess carbon on the nickel surface leads to encapsulation of the nickel particle, deactivating the particle for CNF growth. Data in Figs. 3 and 4 and Table 1 show that such a deactivation effect is not yet prominent for the conditions used in this study and CNF deposition comply increase with increase in ethylene concentration. However, since the C-layer underneath the CNF-layer is at most microporous (*i.e.* poresize <2 nm), this material cannot be classified as 'open' catalyst support (in contrast to entangled CNF layers). Therefore, the thickness of this C-layer should not be too large (*i.e.* <2 μm), which motivates why to use 25 vol.% C_2H_4 for further experiments.

Table 1
Amounts of deposited carbon and average diameter of CNFs for different ethylene concentrations (total flow rate = 100 mL/min; *X* vol.% C_2H_4 balanced with N_2).

C_2H_4 concentration [*X* vol.% balanced with N_2]	C-deposition μg C/μg Ni	Avg. CNF diameter[a] [nm]
5	1.4	52
15	4.3	150
25	12.9	100
30	15.7	71

[a] Avg. of ~50 fibers from HR-SEM images.

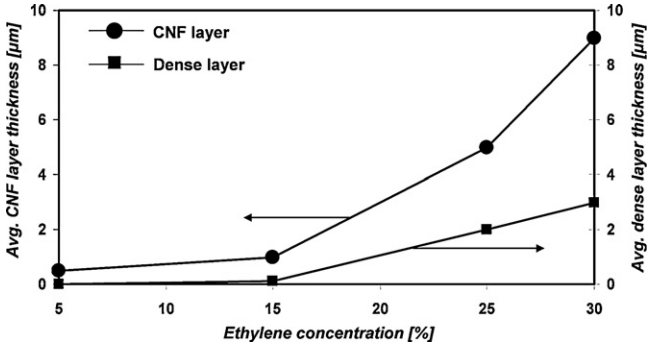

Fig. 4. Influence of the ethylene concentration on the average thicknesses of the CNF layer and the 'dense' C-layer between the CNF layer and the substrate.

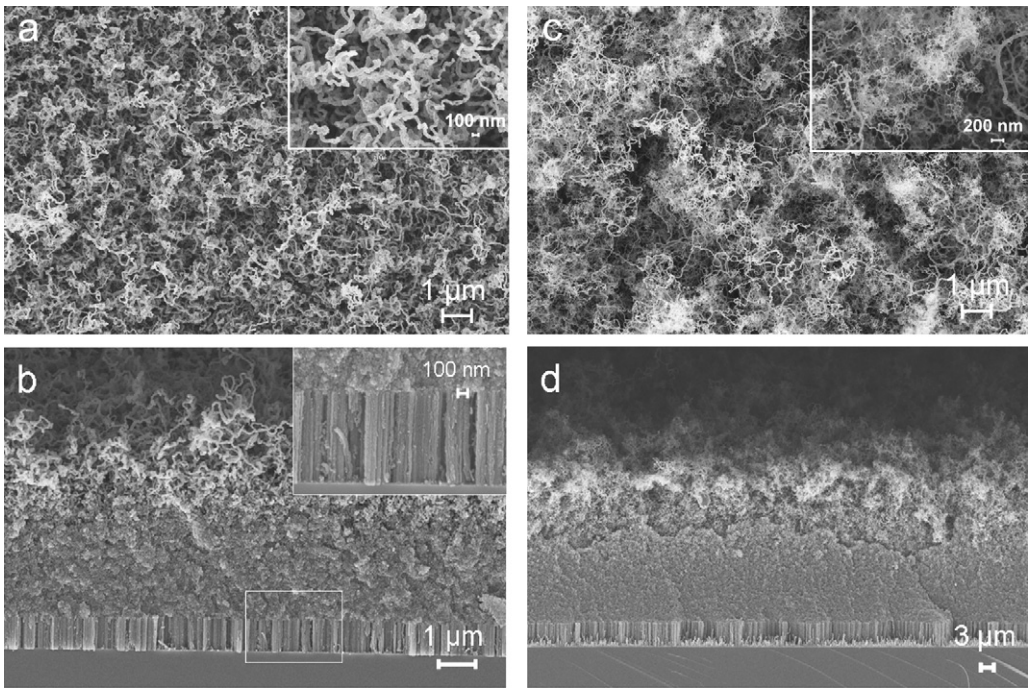

Fig. 5. HR-SEM images illustrating CNF layer morphology for different H_2 concentrations (total flow rate of 100 mL/min; fused silica samples with 25 nm Ni and 10 nm TiW): (a) top-view of CNF layer grown with addition of 6.25 vol.% H_2 (H_2:C_2H_4 = 1:4, v/v); Inset: higher magnification image of CNFs, (b) cross-sectional view of this CNF layer (inset: CNF layer with vertical alignment), (c) top-view of CNF layer grown with addition of 25 vol.% H_2 (H_2:C_2H_4 = 1:1, v/v); Inset: higher magnification image of CNFs, and (d) cross-sectional view of this CNF layer.

3.1.2. Addition of hydrogen during CNF growth

Ni/TiW thin-film samples exposed to the C-TCVD synthesis process during which H_2 was added to the reacting mixture contained significantly thicker CNF layers. This is clearly visible from SEM images (Fig. 5). From the cross-sections it can also be seen that the overall morphology of the CNF layer has changed: underneath the 'open' entangled jungle of CNFs a dense(r) but amorphous C-layer can be distinguished, of which the porosity is (much) lower than of the CNF layer. Furthermore, near the metal surface a dense but rather ordered C-layer is visible, with a nearly vertical alignment of the carbon material. The morphology of this material is very similar to tungsten oxide nanowires synthesized on W-based thin-films with a similar C-TCVD process [61], as a consequence of which it is assumed that the structured layer visible near the metal interface is composed of tungsten-based species.

Fig. 6 shows the thicknesses of the CNF-coating and the dense C-layer (summation of the amorphous and ordered sublayers) as a function of the hydrogen concentration, and Table 2 contains the amounts of deposited carbon and average CNF diameter. It is well known that addition of hydrogen during CNF-synthesis affects the carbon yield, as well as the morphology of produced carbon nanostructures [62–64]. Hydrogen is usually added to slow down the hydrocarbon decomposition, and to achieve better control on carbon formation by rehydrogenating the reactive carbon species in the gas phase as well as reduction of the formation of undesired carbon deposits from the pyrolysis of the carbon feedstock [57]. Due to a lower deactivation rate it also results in higher yields of carbon, resulting in the formation of longer fibers. Data on the amount of deposited carbon (Table 2) and Fig. 6 are in agreement with this theory. However, the fact that thick dense C-layers are formed with hydrogen concentrations above 6.25 vol.% (*i.e.* >12 μm) makes CNF-coatings synthesized with high H_2 concentrations unattractive as structured, open catalyst support.

The diameters of fibers constituting the CNF layers decrease with increasing hydrogen content. Park and Baker have suggested that presence of hydrogen in the reactant responsible for inducing reconstruction/fragmentation of the Ni-particles, *i.e.* the generation of a set of smaller particles with faces that favor the precipitation of carbon in the form of graphite: for increasing hydrogen concentrations in the reactant gas, the associated metal particles tend to become progressively more faceted. During this reconstruction

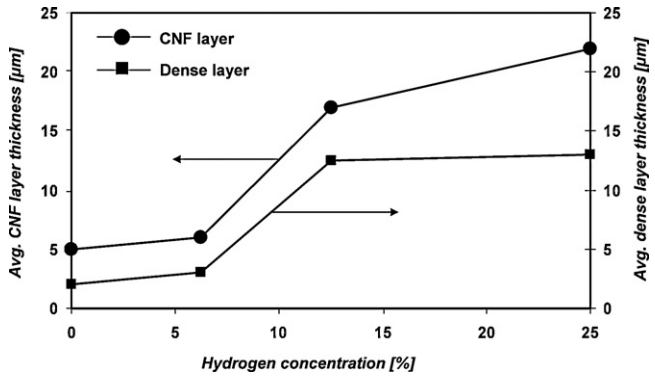

Fig. 6. Influence of the addition of hydrogen to ethylene on the average thicknesses of the CNF layer and 'dense' C-layer(s) between the CNF layer and the substrate.

Table 2
Amounts of deposited carbon and average diameter of CNFs for different hydrogen concentrations (total flow rate = 100 mL/min; *X* vol.% H_2 in 25 vol.% C_2H_4 balanced with N_2).

H_2 concentration [*X* vol.% in 25 vol.% C_2H_4 balanced with N_2]	C-deposition μg C/μg Ni	Avg. CNF diameter[a] [nm]
0[b]	12.9[b]	100[b]
6.25	35.0	47
12.5	65.0	32
25	59.3	17

[a] Avg. of ~50 fibers from HR-SEM images.
[b] Tabulated for comparison (no hydrogen added during CNF growth).

process, the metal particles also undergo a wetting-and-spreading action on graphite at temperatures above 600 °C, *i.e.* incorporation of particles in the fibers. This reconstruction process, thus the formation of smaller metal particles, is responsible for the reduction of the average fiber diameter with increasing hydrogen content [62]. In this work a decrease in carbon yield was found for 25 vol.% H_2 (Table 2), which is in agreement with literature [63,65,66]. This stresses the fact that there is an optimal hydrogen concentration for achieving the maximum growth of CNFs: for Ni/TiW thin-films this is 6.25 vol.% H_2 in 25 vol.% C_2H_4.

The presence of (a) dense C-layer(s) between a layer of entangled CNFs and the fused silica substrate is undesired in case of catalyst support applications, and can be avoided by using Ta as adhesion layer instead of TiW. On fused silica with Ni/Ta no dense C-layers were found for any of the investigated C-TCVD settings as used for Ni/TiW (Fig. 7) [54]. Moreover, CNFs synthesized on Ni/Ta have smaller diameters than CNFs on Ni/TiW (for similar synthesis conditions), resulting in higher surface areas, which is beneficial for the amount of catalytically active species to be anchored to the CNF-based catalyst support.

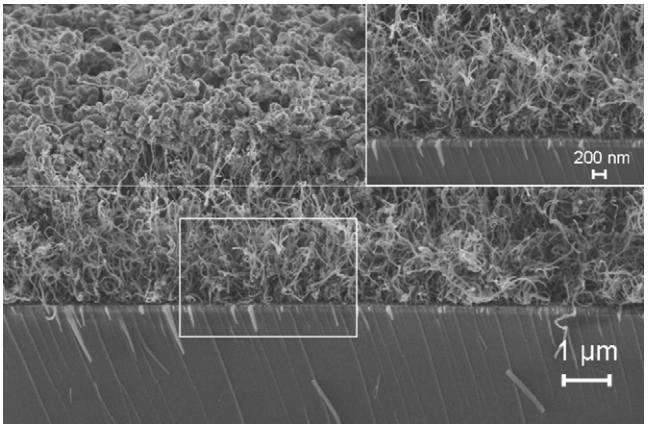

Fig. 7. HR-SEM image showing the morphology of a CNF layer grown on 25 nm Ni and 10 nm Ta on fused silica. Synthesis conditions: 25 vol.% C_2H_4 balanced with N_2 at 700 °C for 1 h, total flow rate 100 mL/min (inset: underneath the CNF layer no dense C-layer(s) are present).

3.1.3. CNF layer synthesis on silicon based flat substrates

Samples with Ni/Ta deposited on oxidized silicon were exposed to the C-TCVD synthesis process. The 'optimal' CNF growth settings as described in Sections 3.1.1 and 3.1.2 were used, *i.e.* 25 vol.% C_2H_4 and at most 6.25 vol.% H_2. Fig. 8a and b show SEM images of a CNF layer grown without hydrogen, and Fig. 8c and d, a CNF layer synthesized with H_2 added to the reaction mixture. There is no noticeable difference in the morphology of CNFs compared to CNFs grown on fused silica, *i.e.* the diameters and CNF layer thicknesses are similar. Moreover, the presence or absence of hydrogen during synthesis affects the CNF layers in an identical way. Chinthaginjala and Lefferts [66] recently published results describing the influence of hydrogen addition on the formation of thin CNF layers on Ni foam material. Although in their case the amount of nickel available for CNF growth is different compared to thin-films used in this work, they have similar observations concerning the change in CNF morphology (*i.e.* their diameter and CNF layer thickness) when hydrogen is present during the growth of CNFs. They indicated that carbon deposition is reduced by adding hydrogen (*i.e.* H_2 suppresses the encapsulation of Ni particles with carbon (which leads to deactivation), thereby obtaining thicker CNF layers), which is in agreement with our results. In addition, they not only observed the formation of thinner fibers on addition of hydrogen to the reaction mixture (which in excellent agreement with our observations), but also concluded this based on BET-measurements: for increasing concentrations of hydrogen the BET-area increased, which is due to increasing amounts of thin fibers. Thus, hydrogen improves the balance between graphene precipitation and carbon deposition in small Ni particles, limiting their encapsulation and extending formation of thin CNFs.

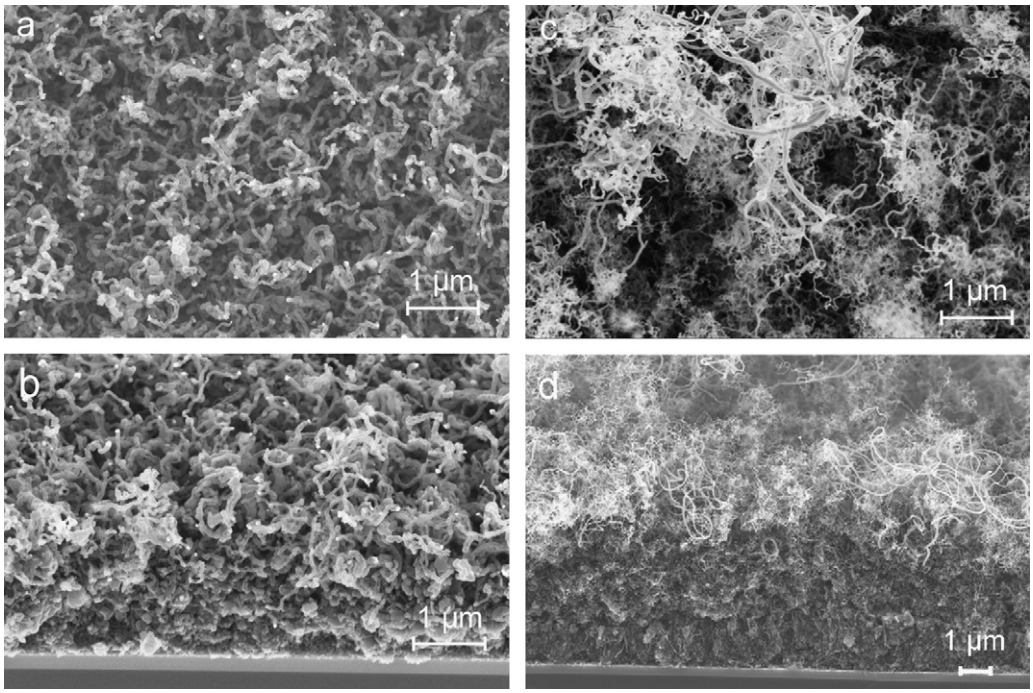

Fig. 8. HR-SEM images illustrating the morphology of a CNF layer grown on 25 nm Ni and 10 nm Ta on oxidized silicon (total flow rate 100 mL/min): CNF layer synthesized without addition of hydrogen to 25 vol.% C_2H_4 (a) top-view, (b) cross-sectional; CNF layer synthesized with 6.25 vol.% H_2 added to 25 vol.% C_2H_4 (H_2:C_2H_4 = 1:1, v/v) (c) top-view, (d) cross-sectional view.

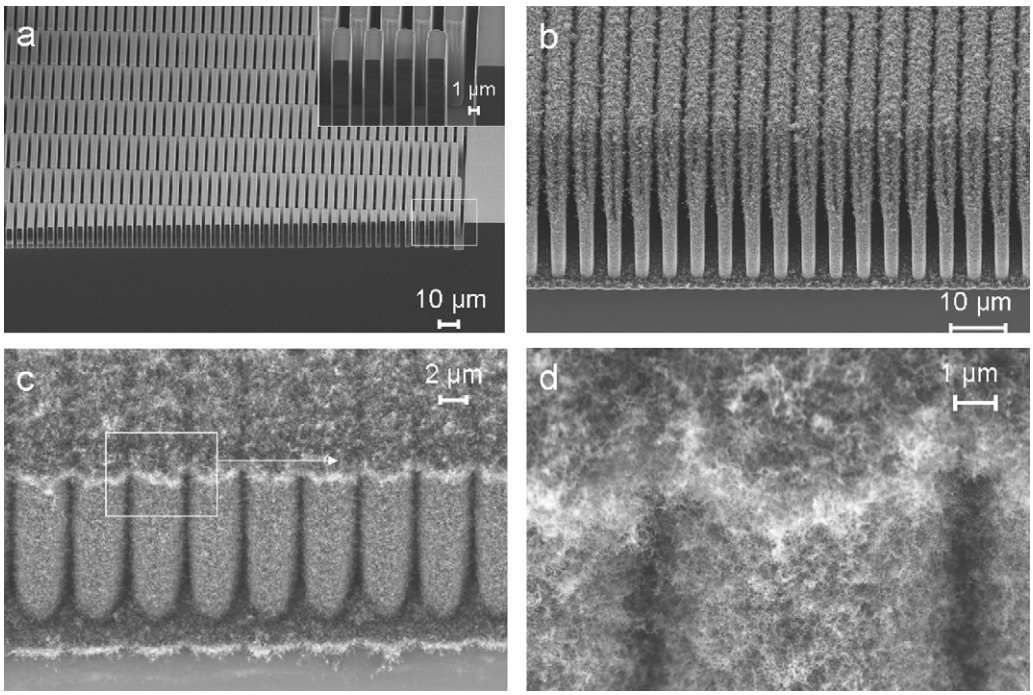

Fig. 9. Cross-sectional SEM images showing arrays of micromachined silicon pillars (a) prior to CNF-synthesis, (b) post to CNF-synthesis without hydrogen (25 vol.% C_2H_4 for 1 h), (c) post to CNF-synthesis with 6.25 vol.% H_2 added to C_2H_4 (growth time 2 h): the CNF layer fills the complete pillar spacing, and (d) the grown CNF-coating exhibits the open structure of entangled CNFs.

The similar results of CNF growth morphology obtained in case of fused silica and oxidized silicon flat substrates show that the morphology of CNF-layers on Ni/Ta and Ni/TiW does not depend on the type of the substrate, which implies that morphological data of CNF-synthesis on flat substrates will be (nearly) similar to morphological properties of CNF-coatings grown on microchannels filled with oxidized silicon pillars.

3.2. Carbon nanofiber based catalyst supports in microreactors

3.2.1. Microchannels with high specific surface areas

As mentioned earlier microreactors offer high surface-to-volume ratios ($\geq 10^4\ m^2/m^3$) which make them attractive for not only performing reactions that require better heat and mass transfer characteristics, but also for processes that require better interphase contact such as gas–liquid–solid reactions. In general, the surface-to-volume ratio is defined as the ratio of surface area [m^2] (where for example catalyst can be anchored) of a system and its internal (void) volume [m^3] (*i.e.* the amount of volume accessible to liquids/gases). For example, when a change is made from a 30 m^3 stirred vessel to 1 L laboratory reactor, this ratio increases a factor 30. If these macrosystems are changed into a microchannel having fluidic channels with a diameter of 30 μm, this ratio rises by a factor of 3000 [67]. The specific surface area available for catalyst deposition inside microreactors can be further improved by wash-coatings or a layer of porous material [15,16,68,69]. For example, Urbiztondo et al. have reported in their work on the development of microstructured zeolite films as highly accessible catalytic coatings for microreactors, that such coatings can exhibit values of the external surface-to-volume ratio in the 400,000–700,000 m^2/m^3 range depending on the preparation conditions. Roumanie et al. [68] have shown that use of arrays of micropillars in microchannels results in a 13-fold increase of specific wall area. In our case of flow channels filled with hexagonal solid pillars (Fig. 2a), the surface-to-volume ratio is ca. $10^5\ m^2/m^3$. Nevertheless, the use of a microporous catalyst support layer (such as an alumina wash-coat) might cause internal mass transfer problems in microsystems, particularly for reactions involving liquid–solid mass transfer [41]. However, when these pillars are covered with carbon nanofibers, in such a way that the spacing between the pillars is completely filled with 'open' CNFs, remarkable surface-to-volume ratios, up to $10^8\ m^2/m^3$, can be achieved without mass transfer problems. This value is in good agreement with the values estimated by Popp and Schneider [70], who demonstrated the use of a monolithic porous carbon nanotube structure as a chemical reactor that exhibited a surface-to-volume ratio of 5×10^6 to $2 \times 10^7\ m^2/m^3$. Such large surface-to-volume ratios provide a considerably higher catalytic activity per unit volume of the channels (assuming homogeneous distribution of catalytic material on the rigid, open CNF-based catalyst support), without facing any internal diffusion limitations for reactant molecules, or hydrodynamic problems for fluid flow, which is essential for performing gas–liquid–solid reactions in an efficient way.

In this work CNF-based catalyst supports are grown in microchannels with arrays of elongated hexagonal silicon pillars containing a thin-film of Ni/Ta, using the optimal CNF-synthesis parameters described in Section 3.1.

3.2.2. Synthesis of CNFs in microchannels containing arrays of micropillars

Flow channels in silicon containing arrays of oxidized silicon micropillars covered with a thin-film of Ni/Ta were exposed to the C-TCVD CNF-synthesis process. Fig. 9a and b show cross-sectional SEM images of micropillars prior and post to a CNF growth procedure using 25 vol.% C_2H_4 for 1 h. The entangled morphology of the CNFs is visible, however, the thickness of the CNF layer is not uniform across the height of the pillars. This non-uniformity can be prevented (to a large extent) by adding hydrogen to the reaction mixture, combined with a larger growth time. In Fig. 9c and d SEM images are shown for a growth procedure using 25 vol.% C_2H_4 with 6.25 vol.% H_2 and a growth time of 2 h. The thickness of the CNF layer is uniform over the height of the pillars. Furthermore,

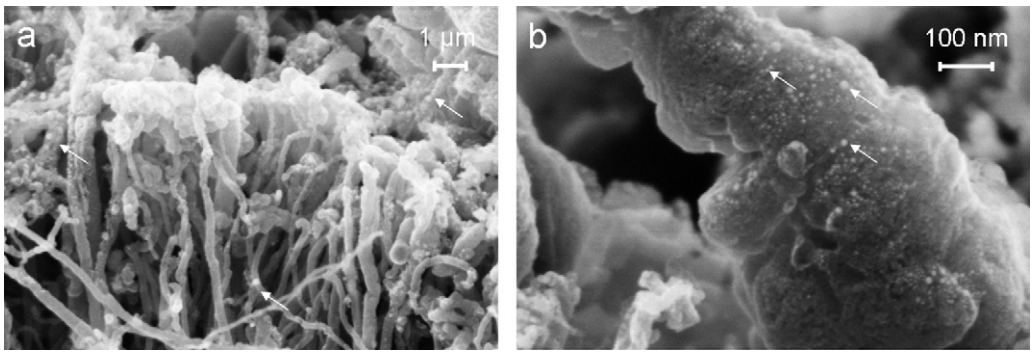

Fig. 10. HR-SEM images of Pt-particles deposited onto CNFs: (a) the particles are uniformly distributed of along the thickness of the CNF layer, and (b) well dispersed Pt catalyst particles (5–10 nm) cover each fiber (Pt-particles are white spots, and are indicated by arrows).

the addition of hydrogen and lengthened growth time resulted in (nearly) complete filling of the pillar spacing, and the CNF layer maintained its open structure.

The thickness non-uniformity of the CNF layer across the height of the micropillars (as seen in Fig. 9b) is a consequence of two issues. Firstly, the (rather) mono-directional origin of the used metal deposition technique plays a role. Like any other PVD-deposition technique, electron-beam evaporation is subject to the 'cosine effect' [71], which means that more material is deposited on planes facing the vapor flux (*i.e.* planes perpendicular to the flux), than on inclined planes (*i.e.* planes non-perpendicular to the flux). In fact, due to this effect a metal film deposited on the sidewall of a trench exhibits a thickness gradient: near the top of the trench the layer is thicker than on the sidewalls in deeper areas of the trench, as well as on the bottom of the trench [72]. For Ni deposited in a microchannel filled with arrays of pillars this implies that the metal layer thickness on top of the pillars will be thicker than the layers at the bottom of the trench and at the sidewalls of the pillars. Moreover, the metal film at the sidewalls of the pillars will have a thickness gradient: the thickness will reduce towards deeper areas of the channel. Since the thickness of the Ni-layer affects the growth rate of CNFs [55], this will result in a CNF layer thickness non-uniformity on the pillar sidewalls.

Secondly, gradients in the hydrocarbon gas across the depth of the microchannel due to close packing of the micropillars can negatively affect the CNF growth rate at deeper areas of the channel. For high-aspect ratio arrays, *i.e.* high pillars with small spacing, gas diffusion limitations can become an issue during CNF growth, similar to gas diffusion problems that occur during deep reactive ion etching of narrow, deep trenches [73].

The presented non-uniformity of the CNF-layer on the pillar sidewalls (Fig. 9b) can be reduced/avoided by increasing the pillar spacing, reduction of the pillar height/channel depth, or by using deposition technique other than conventional PVD-techniques (*i.e.* more multi-directional methods). However, for the pillar array configuration used in this work, the CNF-thickness uniformity can also be significantly improved by adding hydrogen to the hydrocarbon source (as shown in Fig. 9c and d).

3.3. Deposition of catalytic active metal sites on CNF layers

In order to use CNF-layers as efficient, rigid catalyst supports, it is essential to anchor catalytic sites to the fiber bodies, such as metal particles of platinum (Pt). In this work pulsed-laser deposition is used to deposit a Pt thin-film on CNFs synthesized on silicon-based substrates. Post to PLD the samples were annealed at 500 °C in nitrogen for 2 h to generate Pt nanoparticles. Fig. 10 shows high-resolution SEM images of a CNF-layer with Pt-particles attached to the fibers: well-distributed Pt-particles with a size distribution from 5 to 10 nm are visible as white dots (indicated by arrows).

For the application of CNFs as a structured catalyst support in the aqueous phase, modification (and control) of the surface hydrophobicity of the fibers is crucial. It is important to increase the hydrophilicity of the fibers, which can be obtained by oxidation of the surface of the fibers (*e.g.* by immersion in HNO_3, HNO_3/H_2SO_4 or H_2O_2), in order to increase the amount of oxygen containing groups such as carboxylic acid functional groups [74]. The presence of these groups also helps to obtain a higher degree of dispersion of the active phase, particularly when the catalyst preparation will be performed *via* conventional aqueous phase catalyst preparation methods, such as impregnation and/or homogeneous deposition precipitation. A comparative study of the use of these catalyst preparation methods for CNF-based supports is currently examined.

4. Conclusions and outlook

In this work the synthesis and characterization of carbon nanofiber (CNF) layers on nickel-based thin-films is described. By means of high-resolution SEM imaging the influence of various growth parameters on the morphology of catalytic thermal chemical vapor deposited CNF-coatings is studied.

It was found that the most important parameters are the variation in ethylene concentration and addition of hydrogen to the reactant mixture. In case of Ni/TiW and Ni/Ta thin-films (25 nm Ni, 10 nm TiW or Ta) on flat fused silica or oxidized silicon substrates, open, entangled 'jungle' CNF layers were found for ethylene concentrations $\geq$25 vol.%. Moreover, addition of hydrogen to ethylene significantly enhances the rate of formation of CNFs, and reduces the average diameter of the fibers. When TiW is used as adhesion material for Ni, the concentrations of ethylene and hydrogen should not exceed 25 vol.% and 6.25 vol.%, respectively, in order to avoid the existence of a thick 'dense' C-layers between the substrate and the 'open' CNF layer. However, for similar synthesis conditions this C-layer is absent when Ta is used as adhesion material.

CNF-layers are to be used as structured catalyst support in microreactors. The 'optimal' C-TCVD conditions (25 vol.% C_2H_4 with 6.25 vol.% H_2 and a Ni/Ta thin-film) resulted in a good thickness uniformity of CNFs synthesized on the sidewalls of oxidized silicon micropillar arrays. The CNF layers filled up the complete space between the pillars, which is important for performing gas–liquid–solid reactions. Catalytic metal particles were successfully pulsed laser deposited on such rigid, open-structure CNF-coatings, and the particles were homogeneously dispersed over the complete CNF layer. Despite the visually 'open, entangled jungle' character of the CNF layer and the homogeneous distribution of the nanoparticles across its thickness, prior to use of functionalized CNFs in microreactors issues as heat and mass trans-

fer and pressure drops need to be verified experimentally. These aspects are currently being investigated for gas-saturated liquid reactions with Ru/Pd anchored to the CNF-layer.

Acknowledgements

This work was performed with the financial support from MicroNed program, under cluster-II of Smart Microchannel technology (SMACT) and work package II-G-2 and 3 (Smart Micro Reactors). The authors gratefully acknowledge M. Smithers for SEM analysis, and B. Geerdink for technical support. Minh Duc Nguyen (Inorganic Materials Science group, University of Twente, Enschede, The Netherlands) is acknowledged for performing pulsed-laser deposition experiments.

References

[1] W. Ehrfeld, V. Hessel, H. Lowe, Microreactors—New Technology for Modern Chemistry, first ed., Wiley-VCH, Weinheim, 2000.
[2] G. Kolb, V. Hessel, Micro-structured reactors for gas phase reactions, Chem. Eng. J. 98 (2004) 1–38.
[3] H. Lowe, W. Ehrfeld, State-of-the-art in microreaction technology: concepts, manufacturing and applications, Electrochim. Acta 44 (1999) 3679–3689.
[4] M.T. Kreutzer, A. Gunther, Fluid–fluid and fluid–solid mass transfer, in: V. Hessel, A. Renken, J.C. Schouten, J. Yoshida (Eds.), Micro Process Engineering—A Comprehensive Handbook, WILEY-VCH, 2009, pp. 303–322.
[5] L. Kiwi-Minsker, A. Renken, Microstructured reactors for catalytic reactions, Catal. Today 110 (2005) 2–14.
[6] J. Kobayashi, Y. Mori, K. Okamoto, R. Akiyama, M. Ueno, T. Kitamori, S. Kobayashi, A microfluidic device for conducting gas–liquid–solid hydrogenation reactions, Science 304 (2004) 1305–1308.
[7] J. Kobayashi, Y. Mori, S. Kobayashi, Multiphase organic synthesis in microchannel reactors, Chem. - Asian J. 1 (2006) 22–35.
[8] A. Gavriilidis, P. Angeli, Mixing, Contacting of heterogeneous systems, in: V. Hessel, A. Renken, J.C. Schouten, J. Yoshida (Eds.), Micro Process Engineering—A Comprehensive Handbook, WILEY-VCH, 2009, pp. 205–251.
[9] S.K. Ajmera, C. Delattre, M.A. Schmidt, K.F. Jensen, Microreactors for measuring catalyst activity and determining reaction kinetics, Stud. Surf. Sci. Catal. 145 (2003) 97–102.
[10] C.D. Baertsch, M.A. Schmidt, K.F. Jensen, Catalyst surface characterization in microfabricated reactors using pulse chemisorption, Chem. Commun. (2004) 2610–2611.
[11] K. Shah, R.S. Besser, Development of an integrated silicon micro methanol steam reformer to understand thermal management issues in micro fuel processor, in: AIChE Annu. Meet., Conf. Proc., Cincinnati, OH, United States, Oct. 30–Nov. 4, 2005, 2005, 36b/31–36b/38.
[12] V. Meille, Review on methods to deposit catalysts on structured surfaces, Appl. Catal. A 315 (2006) 1–17.
[13] K. Haas-Santo, O. Gorke, P. Pfeifer, K. Schubert, Catalyst coatings for microstructure reactors, Chimia 56 (2002) 605–610.
[14] K. Haas-Santo, M. Fichtner, K. Schubert, Preparation of microstructure compatible porous supports by sol-gel synthesis for catalyst coatings, Appl. Catal. A 220 (2001) 79–92.
[15] J.C. Ganley, E.G. Seebauer, R.I. Masel, Porous anodic alumina microreactors for production of hydrogen from ammonia, AIChE J. 50 (2004) 829–834.
[16] S.R. Deshmukh, A.B. Mhadeshwar, D.G. Vlachos, Microreactor modeling for hydrogen production from ammonia decomposition on ruthenium, Ind. Eng. Chem. Res. 43 (2004) 2986–2999.
[17] V. Sebastian, O. de la Iglesia, R. Mallada, L. Casado, G. Kolb, V. Hessel, J. Santamaria, Preparation of zeolite films as catalytic coatings on microreactor channels, Microporous Mesoporous Mater. 115 (2008) 147–155.
[18] E.V. Rebrov, M.J.M. Mies, M.H.J.M. de Croon, J.C. Schouten, Hydrothermal synthesis of zeolitic coatings for applications in micro-structured reactors, in: V. Valtchev, S. Mintova, M. Tsapatsis (Eds.), Ordered Porous Solids, Elsevier: Amsterdam, 2009, pp. 311–334.
[19] M. Rournanie, C. Delattre, F. Mittler, G. Marchand, V. Meille, C. de Bellefon, C. Pijolat, G. Tournier, P. Pouteau, Enhancing surface activity in silicon microreactors: use of black silicon and alumina as catalyst supports for chemical and biological applications, Chem. Eng. J. 135 (2008) S317–S326.
[20] M.W. Losey, R.J. Jackman, S.L. Firebaugh, M.A. Schmidt, K.F. Jensen, Design and fabrication of microfluidic devices for multiphase mixing and reaction, J. Microelectromech. Syst. 11 (2002) 709–717.
[21] S. Iijima, Helical microtubules of graphitic carbon, Nature 354 (1991) 56–58.
[22] M. Bockrath, D.H. Cobden, P.L. McEuen, N.G. Chopra, A. Zettl, A. Thess, R.E. Smalley, Single-electron transport in ropes of carbon nanotubes, Science 275 (1997) 1922–1925.
[23] M.M.J. Treacy, T.W. Ebbesen, J.M. Gibson, Exceptionally high Young's modulus observed for individual carbon nanotubes, Nature 381 (1996) 678–680.
[24] M.F. Yu, O. Lourie, M.J. Dyer, K. Moloni, T.F. Kelly, R.S. Ruoff, Strength and breaking mechanism of multiwalled carbon nanotubes under tensile load, Science 287 (2000) 637–640.
[25] S.J. Tans, M.H. Devoret, H.J. Dai, A. Thess, R.E. Smalley, L.J. Geerligs, C. Dekker, Individual single-wall carbon nanotubes as quantum wires, Nature 386 (1997) 474–477.
[26] S.S. Fan, M.G. Chapline, N.R. Franklin, T.W. Tombler, A.M. Cassell, H.J. Dai, Self-oriented regular arrays of carbon nanotubes and their field emission properties, Science 283 (1999) 512–514.
[27] E. Hammel, X. Tang, M. Trampert, T. Schmitt, K. Mauthner, A. Eder, P. Potschke, Carbon nanofibers for composite applications, Carbon 42 (2004) 1153–1158.
[28] A.C. Dillon, K.M. Jones, T.A. Bekkedahl, C.H. Kiang, D.S. Bethune, M.J. Heben, Storage of hydrogen in single-walled carbon nanotubes, Nature 386 (1997) 377–379.
[29] W.J. Huang, S. Taylor, K.F. Fu, Y. Lin, D.H. Zhang, T.W. Hanks, A.M. Rao, Y.P. Sun, Attaching proteins to carbon nanotubes via diimide-activated amidation, Nano Lett. 2 (2002) 311–314.
[30] J. Kong, N.R. Franklin, C.W. Zhou, M.G. Chapline, S. Peng, K.J. Cho, H.J. Dai, Nanotube molecular wires as chemical sensors, Science 287 (2000) 622–625.
[31] A.M. Fennimore, T.D. Yuzvinsky, W.Q. Han, M.S. Fuhrer, J. Cumings, A. Zettl, Rotational actuators based on carbon nanotubes, Nature 424 (2003) 408–410.
[32] S.J. Tans, A.R.M. Verschueren, C. Dekker, Room-temperature transistor based on a single carbon nanotube, Nature 393 (1998) 49–52.
[33] C. Wang, M. Waje, X. Wang, J.M. Tang, R.C. Haddon, Y.S. Yan, Proton exchange membrane fuel cells with carbon nanotube based electrodes, Nano Lett. 4 (2004) 345–348.
[34] D. Villers, S.H. Sun, A.M. Serventi, J.P. Dodelet, S. Desilets, Characterization of Pt nanoparticles deposited onto carbon nanotubes grown on carbon paper and evaluation of this electrode for the reduction of oxygen, J. Phys. Chem. B 110 (2006) 25916–25925.
[35] C. Pham-Huu, N. Keller, L.J. Charbonniere, R. Ziessle, M.J. Ledoux, Carbon nanofiber supported palladium catalyst for liquid-phase reactions. An active and selective catalyst for hydrogenation of C=C bonds, Chem. Commun. (2000) 1871–1872.
[36] P. Serp, M. Corrias, P. Kalck, Carbon nanotubes and nanofibers in catalysis, Appl. Catal. A 253 (2003) 337–358.
[37] M.J. Ledoux, C. Pham-Huu, Carbon nanostructures with macroscopic shaping for catalytic applications, Catal. Today 102 (2005) 2–14.
[38] N. Jarrah, J.G. van Ommen, L. Lefferts, Development of monolith with a carbon-nanofiber-washcoat as a structured catalyst support in liquid phase, Catal. Today 79 (2003) 29–33.
[39] N.A. Jarrah, F.H. Li, J.G. van Ommen, L. Lefferts, Immobilization of a layer of carbon nanofibres (CNFs) on Ni foam: a new structured catalyst support, J. Mater. Chem. 15 (2005) 1946–1953.
[40] A. Cordier, E. Flahaut, C. Viazzi, C. Laurent, A. Peigney, In situ CCVD synthesis of carbon nanotubes within a commercial ceramic foam, J. Mater. Chem. 15 (2005) 4041–4050.
[41] P.W.A.M. Wenmakers, J. van der Schaaf, B.F.M. Kuster, J.C. Schouten, "Hairy Foam": carbon nanofibers grown on solid carbon foam. A fully acessible, high surface area, graphitic catalyst support, J. Mater. Chem. 18 (2008) 2426–2436.
[42] P. Tribolet, L. Kiwi-Minsker, Carbon nanofibers grown on metallic filters as novel catalytic materials, Catal. Today 102 (2005) 15–22.
[43] Z.R. Ismagilov, N.V. Shikina, V.N. Kruchinin, N.A. Rudina, V.A. Ushakov, N.T. Vasenin, H.J. Veringa, Development of methods of growing carbon nanofibers on silica glass fiber supports, Catal. Today 102–103 (2005) 85–93.
[44] S.S. Tzeng, K.H. Hung, T.H. Ko, Growth of carbon nanofibers on activated carbon fiber fabrics, Carbon 44 (2006) 859–865.
[45] M. Cantoro, V.B. Golovko, S. Hofmann, D.R. Williams, C. Ducati, J. Geng, B.O. Boskovic, B. Kleinsorge, D.A. Jefferson, A.C. Ferrari, B.F.G. Johnson, J. Robertson, Wet catalyst assisted growth of carbon nanofibers on complex three-dimensional substrates, Diamond Relat. Mater. 14 (2005) 733–738.
[46] T.W. Ebbesen, P.M. Ajayan, Large-scale synthesis of carbon nanotubes, Nature 358 (1992) 220–222.
[47] A. Thess, R. Lee, P. Nikolaev, H.J. Dai, P. Petit, J. Robert, C.H. Xu, Y.H. Lee, S.G. Kim, A.G. Rinzler, D.T. Colbert, G.E. Scuseria, D. Tomanek, J.E. Fischer, R.E. Smalley, Crystalline ropes of metallic carbon nanotubes, Science 273 (1996) 483–487.
[48] V. Ivanov, J.B. Nagy, P. Lambin, A. Lucas, X.B. Zhang, X.F. Zhang, D. Bernaerts, G. Vantendeloo, S. Amelinckx, J. Vanlanduyt, The study of carbon nanotubules produced by catalytic method, Chem. Phys. Lett. 223 (1994) 329–335.
[49] A.V. Melechko, V.I. Merkulov, T.E. McKnight, M.A. Guillorn, K.L. Klein, D.H. Lowndes, M.L. Simpson, Vertically aligned carbon nanofibers and related structures: controlled synthesis and directed assembly, J. Appl. Phys. 97 (2005), -041301.
[50] C.S. Cojocaru, A. Senger, F. Le Normand, A nucleation and growth model of vertically-oriented carbon nanofibers or nanotubes by plasma-enhanced catalytic chemical vapor deposition, J. Nanosci. Nanotechnol. 6 (2006) 1331–1338.
[51] K.P. De Jong, J.W. Geus, Carbon nanofibers: catalytic synthesis and applications, Catal. Rev. -Sci. Eng. 42 (2000) 481–510.
[52] M.L. Toebes, Y.H. Zhang, J. Hajek, T.A. Nijhuis, J.H. Bitter, A.J. van Dillen, D.Y. Murzin, D.C. Koningsberger, K.P. de Jong, Support effects in the hydrogenation of cinnamaldehyde over carbon nanofiber-supported platinum catalysts: characterization and catalysis, J. Catal. 226 (2004) 215–225.
[53] Z.X. Yu, D. Chen, B. Totdal, T.J. Zhao, Y.C. Dai, W.K. Yuan, A. Holmen, Catalytic engineering of carbon nanotube production, Appl. Catal. A 279 (2005) 223–233.
[54] D.B. Thakur, R.M. Tiggelaar, J.G.E. Gardeniers, L. Lefferts, K. Seshan, Growth of carbon nanofiber coatings on nickel thin films on fused silica by catalytic thermal chemical vapor deposition: on the use of titanium, titanium-tungsten and tantalum as adhesion layers, Surf. Coat. Technol. 203 (2009) 3435–3441.

[55] D.B. Thakur, R.M. Tiggelaar, J.G.E. Gardeniers, K. Seshan, L. Lefferts, Synthesis of carbon nanofibers as support layer for metal catalyst in a microreactor for three-phase reactions, Adv. Sci. Technol. 54 (2008) 231–236.
[56] I. Kvande, D. Chen, Z. Yu, M. Ronning, A. Holmen, Optimization and scale-up of CNF production based on intrinsic kinetic data obtained from TEOM, J. Catal. 256 (2008) 204–214.
[57] K.B.K. Teo, C. Singh, M. Chhowalla, W.I. Milne, Catalytic synthesis of carbon nanotubes and nanofibers, in: H.S. Nalwa (Ed.), Encyclopedia of Nanoscience and Nanotechnology, American Scientific Publishers, 2004, pp. 665–686.
[58] J.L. Chen, Y.D. Li, Y.M. Ma, Y.N. Qin, L. Chang, Formation of bamboo-shaped carbon filaments and dependence of their morphology on catalyst composition and reaction conditions, Carbon 39 (2001) 1467–1475.
[59] H. Zhang, G.P. Cao, Z.Y. Wang, Y.S. Yang, Z.J. Shi, Z.N. Gu, Influence of ethylene and hydrogen flow rates on the wall number, crystallinity, and length of millimeter-long carbon nanotube array, J. Phys. Chem. C 112 (2008) 12706–12709.
[60] I. Kvande, G. Oye, N. Hammer, M. Ronning, S. Raaen, A. Holmen, J. Sjoblom, D. Chen, Deposition of Au colloids on plasmachemically modified carbon nanofibers, Carbon 46 (2008) 759–765.
[61] A. Agiral, A.W. Groenland, J.K. Chinthaginjala, K. Seshan, L. Lefferts, J.G.E.H. Gardeniers, On-chip microplasma reactors using carbon nanofibres and tungsten oxide nanowires as electrodes, J. Phys. D: Appl. Phys. 41 (2008) - 194009.
[62] C. Park, R.T.K. Baker, Carbon deposition on iron-nickel during interaction with ethylene-hydrogen mixtures, J. Catal. 179 (1998) 361–374.
[63] C. Pham-Huu, N. Keller, V.V. Roddatis, G. Mestl, R. Schlogl, M.J. Ledoux, Large scale synthesis of carbon nanofibers by catalytic decomposition of ethane on nickel nanoclusters decorating carbon nanotubes, Phys. Chem. Chem. Phys. 4 (2002) 514–521.
[64] Z.X. Yu, D. Chen, B. Totdal, A. Holmen, Parametric study of carbon nanofiber growth by catalytic ethylene decomposition on hydrotalcite derived catalysts, Mater. Chem. Phys. 92 (2005) 71–81.
[65] C. Park, R.T.K. Baker, Carbon deposition on iron-nickel during interaction with ethylene-carbon monoxide-hydrogen mixtures, J. Catal. 190 (2000) 104–117.
[66] J.K. Chinthaginjala, L. Lefferts, Influence of hydrogen on the formation of a thin layer of carbon nanofibers on Ni foam, Carbon 47 (2009) 3175–3183.
[67] O. Worz, K.P. Jackel, T. Richter, A. Wolf, Microreactors—a new efficient tool for reactor development, Chem. Eng. Technol. 24 (2001) 138–142.
[68] M. Roumanie, V. Meille, C. Pijolat, G. Tournier, C. de Bellefon, P. Pouteau, C. Delattre, Design and fabrication of a structured catalytic reactor at micrometer scale: example of methylcyclohexane dehydrogenation, Catal. Today 110 (2005) 164–170.
[69] M.A. Urbiztondo, E. Valera, T. Trifonov, R. Alcubilla, S. Irusta, M.P. Pina, A. Rodriguez, J. Santamaria, Development of microstructured zeolite films as highly accessible catalytic coatings for microreactors, J. Catal. 250 (2007) 190–194.
[70] A. Popp, J.J. Schneider, A chip-sized nanoscale monolithic chemical reactor, Angew. Chem. Int. Ed. 47 (2008) 8958–8960.
[71] A.J. Hart, B.O. Boskovic, A.T.H. Chuang, V.B. Golovko, J. Robertson, B.F.G. Johnson, A.H. Slocum, Uniform and selective CVD growth of carbon nanotubes and nanofibres on arbitrarily microstructured silicon surfaces, Nanotechnology 17 (2006) 1397–1403.
[72] T.S. Cale, G.B. Raupp, T.H. Gandy, Free molecular-transport and deposition in long rectangular trenches, J. Appl. Phys. 68 (1990) 3645–3652.
[73] M.J. de Boer, J.G.E. Gardeniers, H.V. Jansen, E. Smulders, M.J. Gilde, G. Roelofs, J.N. Sasserath, M. Elwenspoek, Guidelines for etching silicon MEMS structures using fluorine high-density plasmas at cryogenic temperatures, J. Microelectromech. Syst. 11 (2002) 385–401.
[74] T.G. Ros, A.J. van Dillen, J.W. Geus, D.C. Koningsberger, Surface oxidation of carbon nanofibres, Chem. -Eur. J. 8 (2002) 1151–1162.